A bias-corrected GEMS geostationary satellite product for nitrogen dioxide using machine learning to enforce consistency with the TROPOMI satellite instrument

Yujin J. Oak[1], Daniel J. Jacob[1,2], Nicholas Balasus[1], Laura H. Yang[1], Heesung Chong[3], Junsung Park[3], Hanlim Lee[4], Gitaek T. Lee[5], Eunjo S. Ha[5], Rokjin J. Park[5], Hyeong-Ahn Kwon[6], Jhoon Kim[7]

[1]School of Engineering and Applied Sciences, Harvard University, Cambridge, MA, USA
[2]Department of Earth and Planetary Sciences, Harvard University, Cambridge, MA, USA
[3]Harvard-Smithsonian Center for Astrophysics, Cambridge, MA, USA
[4]Division of Earth Environmental System Science, Major of Spatial Information Engineering, Pukyong National University, Busan, South Korea
[5]School of Earth and Environmental Science, Seoul National University, Seoul, South Korea
[6]Department of Environmental and Energy Engineering, University of Suwon, Suwon, South Korea
[7]Department of Atmospheric Sciences, Yonsei University, Seoul, South Korea

Correspondence to: Yujin J. Oak (yjoak@g.harvard.edu)

1 Introduction

Nitrogen oxides ($NO_x \equiv NO + NO_2$) are reactive trace gases emitted from combustion, lightning, and microbial activity in soils. Emission is mainly as nitrogen oxide (NO) which cycles rapidly with nitrogen dioxide (NO_2). This cycling produces tropospheric ozone (O_3) and oxidation of NO_x produces nitrate particulate matter (PM), with implications for air quality, climate forcing, and nitrogen deposition. Satellite measurements of NO_2 vertical column densities (VCDs) by solar backscatter from polar sun-synchronous low Earth orbit (LEO) have been used extensively to monitor NO_x emissions and their trends worldwide (Martin et al., 2003; Lamsal et al., 2015; Curier et al., 2014; Duncan et al., 2016; Liu et al., 2017) and to improve understanding of NO_x oxidation chemistry (Boersma et al., 2008; Valin et al., 2013; Miyazaki et al., 2017; Beirle and Wagner, 2024).

NO_2 has been measured continuously from LEO since 1995, starting with the Global Ozone Monitoring Experiment (GOME) (Burrows et al., 1999) followed by the operational GOME-2 series (Munro et al., 2016). The Ozone Monitoring Instrument (OMI) was launched in 2004 and is providing global daily continuous data at 13 × 24 km^2 nadir resolution (Levelt et al., 2006). The TROPOspheric Monitoring Instrument (TROPOMI) launched onboard the Sentinel-5 Precursor (S5P) satellite in 2017 improved the resolution to 3.5 × 5.5 km^2 (Veefkind et al., 2012).

OMI and TROPOMI retrievals of NO_2 have been extensively validated using ground-based measurements of NO_2 VCDs from sun-staring Pandora spectrometers and Multi-Axis Differential Optical Absorption Spectroscopy (MAX-DOAS) instruments, and also by intercomparisons with each other (Herman et al., 2019; Pinardi et al., 2020; Wang et al., 2020; Cai et al., 2022; Gu et al., 2023). TROPOMI NO_2 is routinely validated against Pandora, MAX-DOAS, and OMI by the Royal

Netherlands Meteorological Institute (KNMI), showing overall good agreement with a −7% mean bias (Lambert et al., 2023). It has been used to quantify NO_x emissions (Goldberg et al., 2019), infer surface NO_2 concentrations (Cooper et al., 2020), and evaluate air quality models (Douros et al., 2023).

A limitation with polar sun-synchronous LEO satellites is that they observe a given location at most once per day and at the same time of day. Geostationary satellites can observe at much higher frequency and in principle continuously, providing much denser data and a unique capability for tracking the diurnal cycle of emissions, oxidation chemistry, and pollutant transport. The Geostationary Environment Monitoring Spectrometer (GEMS) was launched onboard the Korea Aerospace Research Institute GEO-KOMPSAT2B (GK2B) satellite in February 2020, in an equatorial plane at 128.2°-longitude with continuous view of East Asia at 3.5 × 7.7 km^2 pixel resolution over Korea (Kim et al., 2020). It is now providing the first NO_2 observations from geostationary orbit. GEMS is part of a geostationary air quality constellation to include TEMPO over North America launched in April 2023 (Zoogman et al., 2017) and Sentinel-4 over Europe to be launched in 2025 (Ingmann et al., 2012).

As with all satellite observations, GEMS retrievals take some time to mature. NO_2 VCDs (L2 products) are currently retrieved operationally with the version 2.0 algorithm (National Institute of Environmental Research, 2020). Evaluation of the GEMS NO_2 product with four urban Pandora sites in South Korea found an underestimate in South Korea and disagreements in diurnal patterns (Kim et al., 2023). However, the local Pandora data may not be representative of the 3.5 × 7.7 km^2 GEMS pixels particularly in urban environments. GEMS evaluation for China found both high and low biases in comparison with ground-based observations and other satellite products (Li et al., 2023; Zhang et al., 2023). Yang et al. (2024) reprocessed the GEMS NO_2 version 2.0 data with prior NO_2 vertical profiles from the GEOS-Chem chemical transport model (CTM) on a 0.25° × 0.3125° grid and found good agreement with Pandora in Seoul and Beijing including diurnal variations.

Here we introduce a bias-corrected GEMS NO_2 product using machine learning (ML) to minimize the biases between GEMS and TROPOMI, and provide in this manner a more reliable and consistent satellite product for scientific applications and for improving the GEMS retrieval. Although TROPOMI observes over a limited range of solar zenith angles (SZAs) on account of the overpass time at approximately 13:30 local time (LT), it has off-track viewing to ± 50° providing a range of viewing zenith angles (VZAs) to mimic the wider range of SZAs seen by GEMS. The bias-corrected GEMS product combines the high data density of GEMS with the accuracy of TROPOMI demonstrated by extensive validation and algorithm development (Gu et al., 2023; Eskes et al., 2022). Our approach is as follows. First, we adjust for biases caused by different prior information used in the operational L2 retrievals by applying common prior vertical profiles simulated by GEOS-Chem. Second, we train an ML model using GEMS and TROPOMI NO_2 VCDs to minimize differences in collocated data during 2022–2023 using GEMS retrieval parameters as explanatory variables. Third, we apply the trained ML model to the ensemble of GEMS data for July 2022–June 2023, producing a bias-corrected GEMS product which has the temporal coverage of GEMS and is consistent with TROPOMI. We use the ML model to identify the GEMS retrieval parameters

associated with the largest discrepancies with TROPOMI and validate this bias-corrected GEMS product with ground-based observations from the Pandora spectrometers.

2 GEMS, TROPOMI, and Pandora operational products

GEMS is an ultraviolet (UV)-visible (VIS) hyperspectral imaging spectrometer that measures solar backscatter with 0.6 nm spectral resolution over East Asia (5−45° latitude, 75−145° longitude) with 3.5 × 7.7 km^2 pixels at 37.5°-latitude and hourly repeat times (08:45−17:45 LT) (Kim et al., 2020). Total NO_2 slant column densities (SCDs) along the sun-satellite light path are retrieved using differential optical absorption spectroscopy (DOAS) (Platt, 1994) with a fitting window of 432–450 nm (National Institute of Environmental Research 2020b; Kim et al., 2020). We use the operational L2 product from version 2.0 (available online: https://nesc.nier.go.kr/en/html/index.do, last access: 19 January 2024).

TROPOMI is similarly a UV-VIS hyperspectral imaging spectrometer with a full width at half maximum (FWHM) of 0.55 nm. It is a push-broom instrument with a wide swath of ~2600 km and an off-track viewing angle of ± 50° off-nadir, providing global daily viewing once a day at approximately 13:30 LT with 5.5 × 3.5 km^2 nadir spatial resolution. Total NO_2 SCDs are retrieved using DOAS in the 405–465 nm window (van Geffen et al., 2022). Here we use the offline (OFFL) L2 product produced by the KNMI NO_2 processor version 2.4.0 (available online: https://dataspace.copernicus.eu/explore-data/data-collections/sentinel-data/sentinel-5p, last access: 19 January 2024).

Ground-based NO_2 column measurements from Pandora instruments have been widely used to validate satellite retrievals (Park et al., 2022; Kim et al., 2023; Pinardi et al., 2020; Yang et al., 2024). Pandora spectrometers provide direct-sun observations to retrieve ground-based NO_2 VCDs by DOAS using a spectral fitting window of 400–470 nm (Herman et al., 2009). Here we use the L2 total NO_2 VCDs processed by the BlickP software (available online: https://www.pandonia-global-network.org, last access: 19 January 2024) at 15 Pandora stations located in Northeast Asia (China, South Korea, Japan) from the Pandonia Global Network (PGN). We select data with quality flags of 0, 1, 10, or 11, and with SZA ≤ 70°.

3 Reprocessing of GEMS and TROPOMI retrievals to use common vertical profiles

Spectral fitting of satellite solar backscatter observations yields NO_2 SCDs, which must be converted to VCDs (the appropriate geophysical quantity) using air mass factors (AMF = SCD/VCD) (Palmer et al., 2001). Standard retrieval algorithms separate the stratospheric and tropospheric portions of the total VCDs to account for the NO_2 background in the stratosphere from oxidation of nitrous oxide (N_2O) (Bucsela et al., 2013), but this introduces uncertainty related to the stratosphere-troposphere separation (STS) algorithm which may differ between retrievals (Geddes et al., 2018) and leads to ambiguity in the allocation of near-tropopause NO_2 such as from lightning and aircraft (Travis et al., 2016; Dang et al., 2023). Since the stratospheric background component is readily predictable from CTMs such as GEOS-Chem (Knowland et al., 2022) and the spatial structure in the NO_2 column is mainly from the troposphere, the purpose for separating stratosphere

and troposphere is in fact not clear. We focus here on total NO_2 VCDs as most useful for scientific applications and to avoid STS errors.

The AMF from the surface to the top of the atmosphere (TOA) can be decomposed into two parts, scattering weights and vertical shape factors, as follows:

$$\text{AMF} = \int_0^{\text{TOA}} w(z)S(z)dz, \quad (1)$$

where *w(z)* is the scattering weight at altitude *z* measuring the sensitivity of the instrument to NO_2 at altitude *z* as computed by a radiative transfer model (RTM), and *S(z)* is the vertical shape factor of normalized number densities obtained from a CTM. Scattering weights for a given wavelength depend on SZA, VZA, relative azimuth angle, surface albedo, and cloud and aerosol optical depths and vertical distributions (Kwon et al., 2019; Hong et al., 2017). The operational GEMS retrieval algorithm uses a look-up-table (LUT) of pre-calculated scattering weights from the VLIDORT RTM at 441 nm (Spurr and Christi, 2014). TROPOMI retrievals use a LUT from the Doubling-Adding KNMI (DAK) RTM at 437.5 nm (Stammes, 2001).

The vertical shape factor $S(z)$ in Eq. (1) describes how NO_2 is distributed with altitude as determined by emissions, chemistry, and transport. It must be prescribed in the retrieval as independent information. The L2 GEMS and TROPOMI retrievals use normalized partial column densities simulated for the local scene by GEOS-Chem (Bey et al., 2001; Yang et al., 2023) at 0.25° × 0.3125° resolution and TM5-MP (Williams et al., 2017; Bucsela et al., 2013) at 1° × 1° resolution, respectively. To eliminate differences caused by using different vertical shape factors, we replace the profiles in the GEMS and TROPOMI L2 products with identical GEOS-Chem model profiles extending from the surface to the stratopause. Yang et al. (2023) showed that GEOS-Chem successfully reproduces the vertical profiles of NO_2 and their diurnal variations observed over South Korea in the KORUS-AQ aircraft campaign, supporting the use of GEOS-Chem profiles in a common AMF calculation for GEMS and TROPOMI satellite retrievals in East Asia. We use monthly mean hourly profiles from a 0.25° × 0.3125° resolution simulation with GEOS-Chem version 13.0.0 (DOI: 10.5281/zenodo.4618180). Details on model configuration and emissions can be found in Lee et al. (2024).

Scattering weights are not provided in the GEMS L2 NO_2 product, therefore we use scattering weights calculated by VLIDORT using GEMS geometry and atmospheric conditions at 448 nm, which are provided in the GEMS L2 glyoxal product (National Institute of Environmental Research 2020a). The AMF for the GEMS total column can then be calculated using vertical shape factors from GEOS-Chem, following Eq. (1). The TROPOMI L2 product reports averaging kernels $A(z)$, which normalize the scattering weights to the reported AMF (Eskes and Boersma, 2003).

$$A(z) = \frac{w(z)}{\text{AMF}} \quad (2)$$

The AMF for the TROPOMI total column can then be calculated from the GEOS-Chem vertical shape factors as follows:

$$\text{AMF'} = \text{AMF}\int_0^{\text{TOA}} A(z)S(z)dz, \quad (3)$$

where AMF is from the L2 product and AMF' is the reprocessed value using GEOS-Chem vertical shape factors. The TROPOMI product reports $A(z)$ for 34 layers, corresponding to the TM5-MP vertical grid, and we interpolate the values to the 47-layer vertical grid of GEOS-Chem. GEMS pixels with AlgorithmQualityFlags > 112, AMFQualityFlags > 64, FinalAlgorithmFlags > 1, and TROPOMI pixels with qa_value < 0.75 are filtered out as per quality control recommendations. We apply area-weighted regridding to the filtered satellite products and use hourly gridded data at 0.25° × 0.3125° resolution with cloud fraction ≤ 0.3 and SZA ≤ 70° for the remainder of this study.

Figure 1 shows how the reprocessing of AMFs modifies the TROPOMI and GEMS NO_2 VCDs compared to the operational L2 products. In what follows, we denote the operational L2 products as "TROPOMI L2" and "GEMS L2", and the products reprocessed with GEOS-Chem vertical profiles as "Reprocessed TROPOMI" and "Reprocessed GEMS". The reprocessing increases TROPOMI in the Northeast Asia source regions including eastern China, South Korea, and Japan. GEMS decreases over eastern China and increases elsewhere.

Figure 2 compares NO_2 VCDs from the L2 and reprocessed products for the ensemble of GEMS and TROPOMI daily data sampled at the overpass time of TROPOMI. For the L2 products we find a negative normalized mean bias (NMB) of −14% in GEMS compared to TROPOMI due to lower background values, but source regions are higher in GEMS. Reprocessing to common prior profiles greatly reduces GEMS-TROPOMI differences except in the background where some differences increase.

Figure 3a compares the mean seasonal variations of Pandora and satellite NO_2 VCDs averaged over the 15 Pandora stations in Northeast Asia. The VCDs are maximum in winter and minimum in summer, reflecting the lifetime of NO_x against photochemical oxidation. The operational TROPOMI L2 product has a −16% NMB relative to the Pandora data that is reduced to 7% when reprocessed with GEOS-Chem vertical profiles. The operational GEMS L2 product has a 23% NMB relative to Pandora that is reduced to 7% when reprocessed with GEOS-Chem vertical profiles. The reprocessed TROPOMI and GEMS products are in close agreement, in contrast to the large differences between the TROPOMI L2 and GEMS L2 products, showing that much of the discrepancy in the L2 products stem from different vertical shape factors. In the following section we correct the remaining discrepancy using machine learning.

Figures 3b and 3c show the mean diurnal variations in the warm and cold seasons, comparing GEMS and Pandora. The Pandora data in the cold season increase over the course of the day due to daytime emissions, while the data in the warm season are minimum in early afternoon due to chemical loss (Yang et al., 2024). The operational GEMS L2 data feature a midday maximum in the cold season that is not seen in the Pandora data. Our reprocessed product is more consistent with the diurnal variation observed by Pandora. More detailed comparisons of diurnal variations in Pandora and GEMS are presented by Yang et al. (2024) for Beijing and Seoul.

4 Bias correction in GEMS using machine learning

Here we construct a corrected GEMS product by developing an ML model that can predict the differences, Δ(GEMS-TROPOMI), remaining between GEMS and TROPOMI after reprocessing to common vertical profiles. TROPOMI is used as reference because of the greater maturity of its retrieval. The ML model uses as predictors the GEMS NO_2 VCD and the GEMS retrieval parameters provided in the L2 product including effective zenith angle (EZA), relative azimuth angle, aerosol optical depth, aerosol layer height, O_3 column amount, surface reflectance at 440 nm, single scattering albedo, cloud fraction, and cloud top pressure. EZA combines the geometric effects of SZA and VZA on the AMF, as defined by the geometric AMF = sec(EZA) + 1 in the absence of scattering (Palmer et al., 2001):

$$\sec(\mathrm{EZA}) = \sec(\mathrm{SZA}) + \sec(\mathrm{VZA}) - 1. \quad (4)$$

TROPOMI observations are for a single time of day but extend off-track to viewing angles ± 50°, so that the collocated dataset covers EZA values ranging up to 75°. This allows us to build an ML model relevant to GEMS observations at different times of day.

We tested five ensemble method algorithms including both bagging (Random Forest, Extra Tree) and boosting (LightGBM, XGBoost, CatBoost) using the Fast and Lightweight AutoML Library (FLAML) (Wang et al., 2021). We separated collocated Δ(GEMS-TROPOMI) pairs into training (July and October 2022, January and April 2023) and test (rest of the collocated data for July 2022–June 2023) datasets. We trained the models to fit 7,489,498 Δ(GEMS-TROPOMI) pairs (training data) for four months as representative of the four seasons, and found that the LightGBM algorithm has the best performance. We excluded Δ(GEMS-TROPOMI) data lying outside six times the interquartile range (6 × IQR; 0.1% of the training data) to avoid contamination by outliers.

We can determine the contribution of each predictor variable to the model prediction using the SHapley Additive exPlanations (SHAP) analysis with the TreeExplainer method (Lundberg et al., 2020), as shown in Figure 4. The SHAP value can be interpreted as the relative importance of the predictor variable to the bias correction, where negative SHAP values indicate low biases in GEMS, and vice versa. Figure 4a shows that the GEMS NO_2 VCD contributes to the largest corrections, followed by the EZA, while variables related to atmospheric scattering and surface reflectance are less important. Figure 4b shows that the corrections from NO_2 VCD and EZA are strongly non-linear. The NO_2 VCD drives the correction of the low bias in the ocean background and the high bias in polluted regions. EZA drives a correction for high biases at angles exceeding 60°. The dominant corrections from VCD and EZA might be viewed as reflecting a correction from the SCD, as we would have SCD/VCD = sec(EZA) + 1 in the absence of scattering. However, we found that using GEMS SCD as a predictor variable was less successful than using VCD.

Figure 5 compares observed and predicted differences for the test data. We conducted a Z-score transform to correct possible systematic biases associated with the LightGBM algorithm (Belitz and Stackelberg, 2021; Balasus et al., 2023). The R^2 for the ML prediction is 0.51 and the root-mean-square-error (RMSE) is 0.65×10^{15} molecules cm^{-2}, which lies within the

estimated single-retrieval errors of GEMS and TROPOMI NO_2 of 0.15−2.47×10^{15} molecules cm^{-2} (Kim et al., 2020) and approximately 0.5×10^{15} molecules cm^{-2} (Van Geffen et al., 2022), respectively.

We produced a corrected GEMS product for the duration of the GEMS L2 version 2.0 record (November 2020 to present) by subtracting Δ(GEMS-TROPOMI) from the GEMS data previously reprocessed to the GEOS-Chem vertical profiles:

$$GEMS_{corrected} = GEMS - \Delta(GEMS\text{-}TROPOMI). \quad (5)$$

The ML calculation of Δ(GEMS-TROPOMI) requires only GEMS retrieval information and is therefore applied to all GEMS retrievals, not requiring collocation with TROPOMI.

Figure 6 compares TROPOMI, GEMS, and the corrected GEMS NO_2 VCDs for the warm and cold seasons. The corrected GEMS product increases the ocean background in GEMS by up to 200% and decreases VCDs in Central Asia by up to 40%, regardless of season. However, corrections to the GEMS product in the polluted regions in Northeast Asia display different patterns during the warm and cold months. We also see from Figure 2 that the correction successfully reduces remaining residual differences between GEMS and TROPOMI (NMB = 0%) and increases consistency with the observed variability from TROPOMI (R^2 = 0.72).

Figure 7 shows an enlarged view of the Northeast Asia domain along with observations from 15 Pandora stations. In the warm season, GEMS displays consistent 10% negative biases relative to TROPOMI in eastern parts of China and South Korea (Figure 7d), resulting in an upward correction. The GEMS bias in the cold season is much noisier and tends to be positive, resulting in downward correction.

The effect of the correction on the diurnal profiles observed by GEMS at the Pandora sites is shown in Figure 3b−c. The correction in the cold season decreases GEMS by similar increments for all hours of the day, resulting in no change in the diurnal profile. The corrected GEMS agrees better with Pandora. The correction in the warm season decreases GEMS values only in early morning and late afternoon, modifying the diurnal profile, but the comparison to Pandora is ambiguous. The Pandora data, observing the urban cores, may be less representative of the GEMS observations in summer than in winter when the NO_x lifetime is longer and winds are stronger (Yang et al., 2024).

5 Conclusions

We have presented an improved NO_2 vertical column density (VCD) product from the Geostationary Environment Monitoring Spectrometer (GEMS) by calibrating it to TROPOspheric Monitoring Instrument (TROPOMI) with a machine learning (ML) algorithm. A first step was to reprocess both GEMS and TROPOMI datasets to adopt common NO_2 vertical profiles and resulting air mass factors (AMFs) from the GEOS-Chem model. The second step was to correct the residual difference in Δ(GEMS-TROPOMI) with an ML model. The corrected GEMS product preserves the data density of GEMS, providing hourly daytime data over East/South Asia and neighboring oceans, and is consistent with TROPOMI. It is available for the duration of the GEMS record (November 2020 to present).

Reprocessing with a common AMF removed most of the differences between GEMS and TROPOMI operational L2 products. It also resulted in better agreement with the ground-based Pandora observations including for GEMS diurnal profiles. Even after this reprocessing, GEMS displayed low biases compared to TROPOMI in polluted regions of eastern China and South Korea, as well as in the ocean background, and high biases in Central Asia.

We used the LightGBM ML algorithm to correct these remaining biases in GEMS relative to TROPOMI. We trained the ML model to fit collocated Δ(GEMS-TROPOMI) pairs for four months (July and October 2022, January and April 2023) to GEMS NO_2 VCDs and GEMS retrieval parameters. This took advantage of the wide range of TROPOMI viewing angles to train the ML in a manner relevant to GEMS observations at different times of day. The ML was successful in correcting the remaining GEMS differences with TROPOMI. SHAP analysis showed that NO_2 VCD and effective zenith angle (EZA) were the predictor variables associated with largest corrections. ML correction increases the ocean background in GEMS by up to 200% and decreases VCDs in Central Asia by up to 40%. GEMS values in NO_x source regions of eastern China and South Korea increase by ~10% during the warm season but decrease during the cold season, resulting in better agreement with Pandora observations. The GEMS correction in these source regions is similar for all times of day in the cold season, but is largest for early morning and late afternoon in the warm season.

Our corrected GEMS NO_2 product is designed to be consistent with the TROPOMI product, supporting the combined use of both datasets for analyses of East Asia air quality including NO_x emissions and chemistry and their diurnal variations. Our approach of calibrating GEMS NO_2 observations to TROPOMI can be extended to other observed species (such as formaldehyde or glyoxal) and to other geostationary satellite instruments including TEMPO over North America and Sentinel-4 over Europe. This would produce consistent datasets across the geostationary air quality constellation with reference to a common TROPOMI calibration for global observing capability.

Data availability

GEMS L2, TROPOMI L2, and Pandora NO_2 products are available online through https://nesc.nier.go.kr/en/html/index.do, https://dataspace.copernicus.eu/explore-data/data-collections/sentinel-data/sentinel-5p, and https://www.pandonia-global-network.org, respectively. The corrected GEMS product from November 2020 to present will be available on Harvard Dataverse upon publication.

Author contributions

Original draft preparation, data processing, analysis, investigation, and visualization were done by YJO. DJJ and NB contributed to project conceptualization. Review and editing were done by DJJ, NB, HC, RJP, H-AK, and JK. LHY, JP, HL, GTL, and ESH provided additional resources and support in analysis.

Competing interests

The contact author has declared that none of the authors has any competing interests.

Financial support

This research was supported by the Samsung Advanced Institute of Technology.

References

Balasus, N., Jacob, D. J., Lorente, A., Maasakkers, J. D., Parker, R. J., Boesch, H., Chen, Z., Kelp, M. M., Nesser, H., and Varon, D. J.: A blended TROPOMI+GOSAT satellite data product for atmospheric methane using machine learning to correct retrieval biases, Atmos. Meas. Tech. Discuss., 2023, 1-40, 10.5194/amt-2023-47, 2023.

Beirle, S. and Wagner, T.: A new method for estimating megacity NOx emissions and lifetimes from satellite observations, EGUsphere, 2024, 1-21, 10.5194/egusphere-2023-3079, 2024.

Belitz, K. and Stackelberg, P. E.: Evaluation of six methods for correcting bias in estimates from ensemble tree machine learning regression models, Environmental Modelling & Software, 139, 105006, https://doi.org/10.1016/j.envsoft.2021.105006, 2021.

Bey, I., Jacob, D. J., Yantosca, R. M., Logan, J. A., Field, B. D., Fiore, A. M., Li, Q., Liu, H. Y., Mickley, L. J., and Schultz, M. G.: Global modeling of tropospheric chemistry with assimilated meteorology: Model description and evaluation, Journal of Geophysical Research: Atmospheres, 106, 23073-23095, https://doi.org/10.1029/2001JD000807, 2001.

Boersma, K. F., Jacob, D. J., Eskes, H. J., Pinder, R. W., Wang, J., and van der A, R. J.: Intercomparison of SCIAMACHY and OMI tropospheric NO2 columns: Observing the diurnal evolution of chemistry and emissions from space, Journal of Geophysical Research: Atmospheres, 113, https://doi.org/10.1029/2007JD008816, 2008.

Bucsela, E. J., Krotkov, N. A., Celarier, E. A., Lamsal, L. N., Swartz, W. H., Bhartia, P. K., Boersma, K. F., Veefkind, J. P., Gleason, J. F., and Pickering, K. E.: A new stratospheric and tropospheric NO₂ retrieval algorithm for nadir-viewing satellite instruments: applications to OMI, Atmos. Meas. Tech., 6, 2607-2626, 10.5194/amt-6-2607-2013, 2013.

Burrows, J. P., Weber, M., Buchwitz, M., Rozanov, V., Ladstätter-Weißenmayer, A., Richter, A., DeBeek, R., Hoogen, R., Bramstedt, K., Eichmann, K.-U., Eisinger, M., and Perner, D.: The Global Ozone Monitoring Experiment (GOME): Mission Concept and First Scientific Results, Journal of the Atmospheric Sciences, 56, 151-175, https://doi.org/10.1175/1520-0469(1999)056<0151:TGOMEG>2.0.CO;2, 1999.

Cai, K., Li, S., Lai, J., Xia, Y., Wang, Y., Hu, X., and Li, A.: Evaluation of TROPOMI and OMI Tropospheric NO2 Products Using Measurements from MAX-DOAS and State-Controlled Stations in the Jiangsu Province of China, Atmosphere, 13, 886, 2022.

The International GEOS-Chem User Community: geoschem/GCClassic: GEOS-Chem 13.0.0 (13.0.0) [dataset], https://doi.org/10.5281/zenodo.4618180, 2021.

Cooper, M. J., Martin, R. V., McLinden, C. A., and Brook, J. R.: Inferring ground-level nitrogen dioxide concentrations at fine spatial resolution applied to the TROPOMI satellite instrument, Environmental Research Letters, 15, 104013, 10.1088/1748-9326/aba3a5, 2020.

Curier, R. L., Kranenburg, R., Segers, A. J. S., Timmermans, R. M. A., and Schaap, M.: Synergistic use of OMI NO2 tropospheric columns and LOTOS–EUROS to evaluate the NOx emission trends across Europe, Remote Sensing of Environment, 149, 58-69, https://doi.org/10.1016/j.rse.2014.03.032, 2014.

Dang, R., Jacob, D. J., Shah, V., Eastham, S. D., Fritz, T. M., Mickley, L. J., Liu, T., Wang, Y., and Wang, J.: Background nitrogen dioxide (NO2) over the United States and its implications for satellite observations and trends: effects of nitrate photolysis, aircraft, and open fires, Atmos. Chem. Phys., 23, 6271-6284, 10.5194/acp-23-6271-2023, 2023.

Douros, J., Eskes, H., van Geffen, J., Boersma, K. F., Compernolle, S., Pinardi, G., Blechschmidt, A. M., Peuch, V. H., Colette, A., and Veefkind, P.: Comparing Sentinel-5P TROPOMI NO2 column observations with the CAMS regional air quality ensemble, Geosci. Model Dev., 16, 509-534, 10.5194/gmd-16-509-2023, 2023.

Duncan, B. N., Lamsal, L. N., Thompson, A. M., Yoshida, Y., Lu, Z., Streets, D. G., Hurwitz, M. M., and Pickering, K. E.: A space-based, high-resolution view of notable changes in urban NOx pollution around the world (2005–2014), Journal of Geophysical Research: Atmospheres, 121, 976-996, https://doi.org/10.1002/2015JD024121, 2016.

Eskes, H., van Geffen, J., Boersma, F., Eichmann, K.-U., Apituley, A., Pedergnana, M., Sneep, M., Veefkind, J. P., and Loyola, D.: Sentinel-5 precursor/TROPOMI Level 2 Product User Manual Nitrogendioxide, 2022.

Eskes, H. J. and Boersma, K. F.: Averaging kernels for DOAS total-column satellite retrievals, Atmos. Chem. Phys., 3, 1285-1291, 10.5194/acp-3-1285-2003, 2003.

Geddes, J. A., Martin, R. V., Bucsela, E. J., McLinden, C. A., and Cunningham, D. J. M.: Stratosphere–troposphere separation of nitrogen dioxide columns from the TEMPO geostationary satellite instrument, Atmos. Meas. Tech., 11, 6271-6287, 10.5194/amt-11-6271-2018, 2018.

Goldberg, D. L., Lu, Z., Streets, D. G., de Foy, B., Griffin, D., McLinden, C. A., Lamsal, L. N., Krotkov, N. A., and Eskes, H.: Enhanced Capabilities of TROPOMI NO2: Estimating NO_x from North American Cities and Power Plants, Environmental Science & Technology, 53, 12594-12601, 10.1021/acs.est.9b04488, 2019.

Gu, J., Liang, X., Song, S., Tian, Y., Chen, L., and Tao, J.: Evaluation of TROPOMI operational standard NO2 column retrievals (from version 1.3 to 2.4) with OMNO2 and QA4ECV OMI observations over China, EGUsphere, 2023, 1-40, 10.5194/egusphere-2023-175, 2023.

Herman, J., Cede, A., Spinei, E., Mount, G., Tzortziou, M., and Abuhassan, N.: NO2 column amounts from ground-based Pandora and MFDOAS spectrometers using the direct-sun DOAS technique: Intercomparisons and application to OMI validation, Journal of Geophysical Research: Atmospheres, 114, https://doi.org/10.1029/2009JD011848, 2009.

Herman, J., Abuhassan, N., Kim, J., Kim, J., Dubey, M., Raponi, M., and Tzortziou, M.: Underestimation of column NO2 amounts from the OMI satellite compared to diurnally varying ground-based retrievals from multiple PANDORA spectrometer instruments, Atmos. Meas. Tech., 12, 5593-5612, 10.5194/amt-12-5593-2019, 2019.

Hong, H., Lee, H., Kim, J., Jeong, U., Ryu, J., and Lee, D. S.: Investigation of Simultaneous Effects of Aerosol Properties and Aerosol Peak Height on the Air Mass Factors for Space-Borne NO2 Retrievals, Remote. Sens., 9, 208, 2017.

Ingmann, P., Veihelmann, B., Langen, J., Lamarre, D., Stark, H., and Courrèges-Lacoste, G. B.: Requirements for the GMES Atmosphere Service and ESA's implementation concept: Sentinels-4/-5 and -5p, Remote Sensing of Environment, 120, 58-69, https://doi.org/10.1016/j.rse.2012.01.023, 2012.

Kim, J., Jeong, U., Ahn, M.-H., Kim, J. H., Park, R. J., Lee, H., Song, C. H., Choi, Y.-S., Lee, K.-H., Yoo, J.-M., Jeong, M.-J., Park, S. K., Lee, K.-M., Song, C.-K., Kim, S.-W., Kim, Y. J., Kim, S.-W., Kim, M., Go, S., Liu, X., Chance, K., Chan Miller, C., Al-Saadi, J., Veihelmann, B., Bhartia, P. K., Torres, O., Abad, G. G., Haffner, D. P., Ko, D. H., Lee, S. H., Woo, J.-H., Chong, H., Park, S. S., Nicks, D., Choi, W. J., Moon, K.-J., Cho, A., Yoon, J., Kim, S.-k., Hong, H., Lee, K., Lee, H., Lee, S., Choi, M., Veefkind, P., Levelt, P. F., Edwards, D. P., Kang, M., Eo, M., Bak, J., Baek, K., Kwon, H.-A., Yang, J., Park, J., Han, K. M., Kim, B.-R., Shin, H.-W., Choi, H., Lee, E., Chong, J., Cha, Y., Koo, J.-H., Irie, H., Hayashida, S., Kasai, Y., Kanaya, Y., Liu, C., Lin, J., Crawford, J. H., Carmichael, G. R., Newchurch, M. J., Lefer, B. L., Herman, J. R., Swap, R. J., Lau, A. K. H., Kurosu, T. P., Jaross, G., Ahlers, B., Dobber, M., McElroy, C. T., and Choi, Y.: New Era of Air Quality Monitoring from Space: Geostationary Environment Monitoring Spectrometer (GEMS), Bulletin of the American Meteorological Society, 101, E1-E22, https://doi.org/10.1175/BAMS-D-18-0013.1, 2020.

Kim, S., Kim, D., Hong, H., Chang, L. S., Lee, H., Kim, D. R., Kim, D., Yu, J. A., Lee, D., Jeong, U., Song, C. K., Kim, S. W., Park, S. S., Kim, J., Hanisco, T. F., Park, J., Choi, W., and Lee, K.: First-time comparison between NO2 vertical columns from GEMS and Pandora measurements, Atmos. Meas. Tech. Discuss., 2023, 1-22, 10.5194/amt-2023-11, 2023.

Knowland, K. E., Keller, C. A., Wales, P. A., Wargan, K., Coy, L., Johnson, M. S., Liu, J., Lucchesi, R. A., Eastham, S. D., Fleming, E., Liang, Q., Leblanc, T., Livesey, N. J., Walker, K. A., Ott, L. E., and Pawson, S.: NASA GEOS Composition Forecast Modeling System GEOS-CF v1.0: Stratospheric Composition, Journal of Advances in Modeling Earth Systems, 14, e2021MS002852, https://doi.org/10.1029/2021MS002852, 2022.

Kwon, H. A., Park, R. J., González Abad, G., Chance, K., Kurosu, T. P., Kim, J., De Smedt, I., Van Roozendael, M., Peters, E., and Burrows, J.: Description of a formaldehyde retrieval algorithm for the Geostationary Environment Monitoring Spectrometer (GEMS), Atmos. Meas. Tech., 12, 3551-3571, 10.5194/amt-12-3551-2019, 2019.

Lambert, J.-C., Keppens, A., Compernolle, S., Eichmann, K.-U., Graaf, M. d., Hubert, D., Langerock, B., Ludewig, A., Sha, M. K., Verhoelst, T., Wagner, T., Ahn, C., Argyrouli, A., Balis, D., Chan, K. L., Coldewey-Egbers, M., Smedt, I. D., Eskes, H., Fjæraa, A. M., Garane, K., Gleason, J. F., Goutail, F., Granville, J., Hedelt, P., Ahn, C., Heue, K.-P., Jaross, G., Kleipool, Q., Koukouli, M., Lutz, R., Velarte, M. C. M., Michailidis, K., Nanda, S., Niemeijer, S., Pazmiño, A., Pinardi, G., Richter, A., Rozemeijer, N., Sneep, M., Zweers, D. S., Theys, N., Tilstra, G., Torres, O., Valks, P., Geffen, J. v., Vigouroux,

C., Wang, P., and Weber, M.: Quarterly Validation Report of the Copernicus Sentinel-5 Precursor Operational Data Products #21: April 2018 – November 2023., 194, 2023.

Lamsal, L. N., Duncan, B. N., Yoshida, Y., Krotkov, N. A., Pickering, K. E., Streets, D. G., and Lu, Z.: U.S. NO2 trends (2005–2013): EPA Air Quality System (AQS) data versus improved observations from the Ozone Monitoring Instrument (OMI), Atmospheric Environment, 110, 130-143, https://doi.org/10.1016/j.atmosenv.2015.03.055, 2015.

Lee, G. T., Park, R. J., Kwon, H. A., Ha, E. S., Lee, S. D., Shin, S., Ahn, M. H., Kang, M., Choi, Y. S., Kim, G., Lee, D. W., Kim, D. R., Hong, H., Langerock, B., Vigouroux, C., Lerot, C., Hendrick, F., Pinardi, G., De Smedt, I., Van Roozendael, M., Wang, P., Chong, H., Cho, Y., and Kim, J.: First evaluation of the GEMS formaldehyde retrieval algorithm against TROPOMI and ground-based column measurements during the in-orbit test period, EGUsphere, 2023, 1-33, 10.5194/egusphere-2023-1918, 2024.

Levelt, P. F., Oord, G. H. J. v. d., Dobber, M. R., Malkki, A., Huib, V., Johan de, V., Stammes, P., Lundell, J. O. V., and Saari, H.: The ozone monitoring instrument, IEEE Transactions on Geoscience and Remote Sensing, 44, 1093-1101, 10.1109/TGRS.2006.872333, 2006.

Li, Y., Xing, C., Peng, H., Song, Y., Zhang, C., Xue, J., Niu, X., and Liu, C.: Long-term observations of NO2 using GEMS in China: Validations and regional transport, Science of The Total Environment, 904, 166762, https://doi.org/10.1016/j.scitotenv.2023.166762, 2023.

Liu, F., Beirle, S., Zhang, Q., van der A, R. J., Zheng, B., Tong, D., and He, K.: NOx emission trends over Chinese cities estimated from OMI observations during 2005 to 2015, Atmos. Chem. Phys., 17, 9261-9275, 10.5194/acp-17-9261-2017, 2017.

Lundberg, S. M., Erion, G., Chen, H., DeGrave, A., Prutkin, J. M., Nair, B., Katz, R., Himmelfarb, J., Bansal, N., and Lee, S.-I.: From local explanations to global understanding with explainable AI for trees, Nature Machine Intelligence, 2, 56-67, 10.1038/s42256-019-0138-9, 2020.

Martin, R. V., Jacob, D. J., Chance, K., Kurosu, T. P., Palmer, P. I., and Evans, M. J.: Global inventory of nitrogen oxide emissions constrained by space-based observations of NO2 columns, Journal of Geophysical Research: Atmospheres, 108, https://doi.org/10.1029/2003JD003453, 2003.

Miyazaki, K., Eskes, H., Sudo, K., Boersma, K. F., Bowman, K., and Kanaya, Y.: Decadal changes in global surface NOx emissions from multi-constituent satellite data assimilation, Atmos. Chem. Phys., 17, 807-837, 10.5194/acp-17-807-2017, 2017.

Munro, R., Lang, R., Klaes, D., Poli, G., Retscher, C., Lindstrot, R., Huckle, R., Lacan, A., Grzegorski, M., Holdak, A., Kokhanovsky, A., Livschitz, J., and Eisinger, M.: The GOME-2 instrument on the Metop series of satellites: instrument design, calibration, and level 1 data processing – an overview, Atmos. Meas. Tech., 9, 1279-1301, 10.5194/amt-9-1279-2016, 2016.

Palmer, P. I., Jacob, D. J., Chance, K., Martin, R. V., Spurr, R. J. D., Kurosu, T. P., Bey, I., Yantosca, R., Fiore, A., and Li, Q.: Air mass factor formulation for spectroscopic measurements from satellites: Application to formaldehyde retrievals

from the Global Ozone Monitoring Experiment, Journal of Geophysical Research: Atmospheres, 106, 14539-14550, https://doi.org/10.1029/2000JD900772, 2001.

Park, J., Park, J.-S., Santana Díaz, D., Gebetsberger, M., Mueller, M., Shalaby, L., Tiefengraber, M., Kim, H.-J., Park, S. S., Song, C.-K., and Kim, S.-W.: Spatiotemporal inhomogeneity of total column NO 2 in a polluted urban area inferred from TROPOMI and Pandora intercomparisons, GIScience & Remote Sensing, 59, 354-373, 10.1080/15481603.2022.2026640, 2022.

Pinardi, G., Van Roozendael, M., Hendrick, F., Theys, N., Abuhassan, N., Bais, A., Boersma, F., Cede, A., Chong, J., Donner, S., Drosoglou, T., Dzhola, A., Eskes, H., Frieß, U., Granville, J., Herman, J. R., Holla, R., Hovila, J., Irie, H., Kanaya, Y., Karagkiozidis, D., Kouremeti, N., Lambert, J. C., Ma, J., Peters, E., Piters, A., Postylyakov, O., Richter, A., Remmers, J., Takashima, H., Tiefengraber, M., Valks, P., Vlemmix, T., Wagner, T., and Wittrock, F.: Validation of tropospheric NO2 column measurements of GOME-2A and OMI using MAX-DOAS and direct sun network observations, Atmos. Meas. Tech., 13, 6141-6174, 10.5194/amt-13-6141-2020, 2020.

Platt, U.: Differential Optical Absorption Spectroscopy (DOAS), in: Air monitoring by spectroscopic techniques, edited by: Sigrist, M. W., 127, 27–76, https://doi.org/10.1002/9780470027318.a0706, 1994.

National Institute of Environmental Research (NIER).: Geostationary Environment Monitoring Spectrometer (GEMS) Algorithm Theoretical Basis Document VOC (HCHO/CHOCHO) Retrieval Algorithm, 2020a.

National Institute of Environmental Research (NIER).: Geostationary Environment Monitoring Spectrometer (GEMS) Algorithm Theoretical Basis Document NO2 Retrieval Algorithm, 2020b.

Spurr, R. and Christi, M.: On the generation of atmospheric property Jacobians from the (V)LIDORT linearized radiative transfer models, Journal of Quantitative Spectroscopy and Radiative Transfer, 142, 109-115, https://doi.org/10.1016/j.jqsrt.2014.03.011, 2014.

Stammes, P.: Spectral radiance modelling in the UV-visible range, 2001.

Travis, K., Jacob, D., Fisher, J., Kim, P., Marais, E., Zhu, L., Yu, K., Miller, C., Yantosca, R., Sulprizio, M., Thompson, A., Wennberg, P., Crounse, J., Clair, J., Cohen, R., Laughner, J., Dibb, J., Hall, S., Ullmann, K., and Zhou, X.: Why do models overestimate surface ozone in the Southeast United States?, Atmospheric Chemistry and Physics, 16, 13561-13577, 10.5194/acp-16-13561-2016, 2016.

Valin, L. C., Russell, A. R., and Cohen, R. C.: Variations of OH radical in an urban plume inferred from NO2 column measurements, Geophysical Research Letters, 40, 1856-1860, https://doi.org/10.1002/grl.50267, 2013.

van Geffen, J. H. G. M., Eskes, H. J., Boersma, K. F., and Veefkind, J. P.: TROPOMI ATBD of the total and tropospheric NO2 data products, 2022.

Veefkind, J. P., Aben, I., McMullan, K., Förster, H., de Vries, J., Otter, G., Claas, J., Eskes, H. J., de Haan, J. F., Kleipool, Q., van Weele, M., Hasekamp, O., Hoogeveen, R., Landgraf, J., Snel, R., Tol, P., Ingmann, P., Voors, R., Kruizinga, B., Vink, R., Visser, H., and Levelt, P. F.: TROPOMI on the ESA Sentinel-5 Precursor: A GMES mission for

global observations of the atmospheric composition for climate, air quality and ozone layer applications, Remote Sensing of Environment, 120, 70-83, https://doi.org/10.1016/j.rse.2011.09.027, 2012.

Wang, C., Wang, T., Wang, P., and Rakitin, V.: Comparison and Validation of TROPOMI and OMI NO2 Observations over China, Atmosphere, 11, 636, 2020.

Wang, C., Wu, Q., Weimer, M., and Zhu, E.: Flaml: A fast and lightweight automl library, Proceedings of Machine Learning and Systems, 3, 434-447, 2021.

Williams, J. E., Boersma, K. F., Le Sager, P., and Verstraeten, W. W.: The high-resolution version of TM5-MP for optimized satellite retrievals: description and validation, Geosci. Model Dev., 10, 721-750, 10.5194/gmd-10-721-2017, 2017.

Yang, L. H., Jacob, D. J., Colombi, N. K., Zhai, S., Bates, K. H., Shah, V., Beaudry, E., Yantosca, R. M., Lin, H., Brewer, J. F., Chong, H., Travis, K. R., Crawford, J. H., Lamsal, L. N., Koo, J. H., and Kim, J.: Tropospheric NO2 vertical profiles over South Korea and their relation to oxidant chemistry: implications for geostationary satellite retrievals and the observation of NO2 diurnal variation from space, Atmos. Chem. Phys., 23, 2465-2481, 10.5194/acp-23-2465-2023, 2023.

Yang, L. H., Jacob, D. J., Dang, R., Oak, Y. J., Lin, H., Kim, J., Zhai, S., Colombi, N. K., Pendergrass, D. C., Beaudry, E., Shah, V., Feng, X., Yantosca, R. M., Chong, H., Park, J., Lee, H., Lee, W. J., Kim, S., Kim, E., Travis, K. R., Crawford, J. H., and Liao, H.: Interpreting GEMS geostationary satellite observations of the diurnal variation of nitrogen dioxide (NO2) over East Asia, EGUsphere, 2023, 1-25, 10.5194/egusphere-2023-2979, 2024.

Zhang, Y., Lin, J., Kim, J., Lee, H., Park, J., Hong, H., Van Roozendael, M., Hendrick, F., Wang, T., Wang, P., He, Q., Qin, K., Choi, Y., Kanaya, Y., Xu, J., Xie, P., Tian, X., Zhang, S., Wang, S., Spurr, R., Chen, L., Kong, H., and Liu, M.: POMINO-GEMS: A Research Product for Tropospheric NO2 Columns from Geostationary Environment Monitoring Spectrometer, Atmos. Meas. Tech. Discuss., 2023, 1-28, 10.5194/amt-2023-46, 2023.

Zoogman, P., Liu, X., Suleiman, R. M., Pennington, W. F., Flittner, D. E., Al-Saadi, J. A., Hilton, B. B., Nicks, D. K., Newchurch, M. J., Carr, J. L., Janz, S. J., Andraschko, M. R., Arola, A., Baker, B. D., Canova, B. P., Chan Miller, C., Cohen, R. C., Davis, J. E., Dussault, M. E., Edwards, D. P., Fishman, J., Ghulam, A., González Abad, G., Grutter, M., Herman, J. R., Houck, J., Jacob, D. J., Joiner, J., Kerridge, B. J., Kim, J., Krotkov, N. A., Lamsal, L., Li, C., Lindfors, A., Martin, R. V., McElroy, C. T., McLinden, C., Natraj, V., Neil, D. O., Nowlan, C. R., O'Sullivan, E. J., Palmer, P. I., Pierce, R. B., Pippin, M. R., Saiz-Lopez, A., Spurr, R. J. D., Szykman, J. J., Torres, O., Veefkind, J. P., Veihelmann, B., Wang, H., Wang, J., and Chance, K.: Tropospheric emissions: Monitoring of pollution (TEMPO), Journal of Quantitative Spectroscopy and Radiative Transfer, 186, 17-39, https://doi.org/10.1016/j.jqsrt.2016.05.008, 2017.

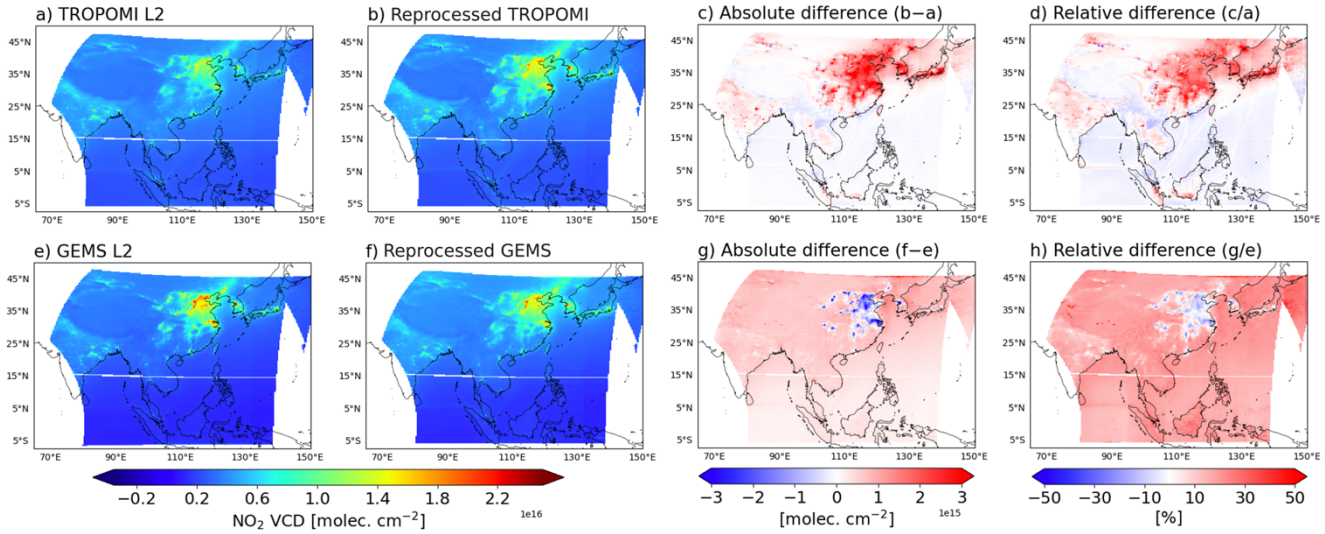

Figure 1: NO_2 vertical column densities (VCDs) from TROPOMI and GEMS. Values are averages for July 2022−June 2023 sampled at the overpass time of TROPOMI (13:30 local time; LT). The top panels show the TROPOMI operational product (L2), our product reprocessed with GEOS-Chem NO_2 vertical profiles, and the absolute and relative differences between the two. The lower panels show the same for GEMS.

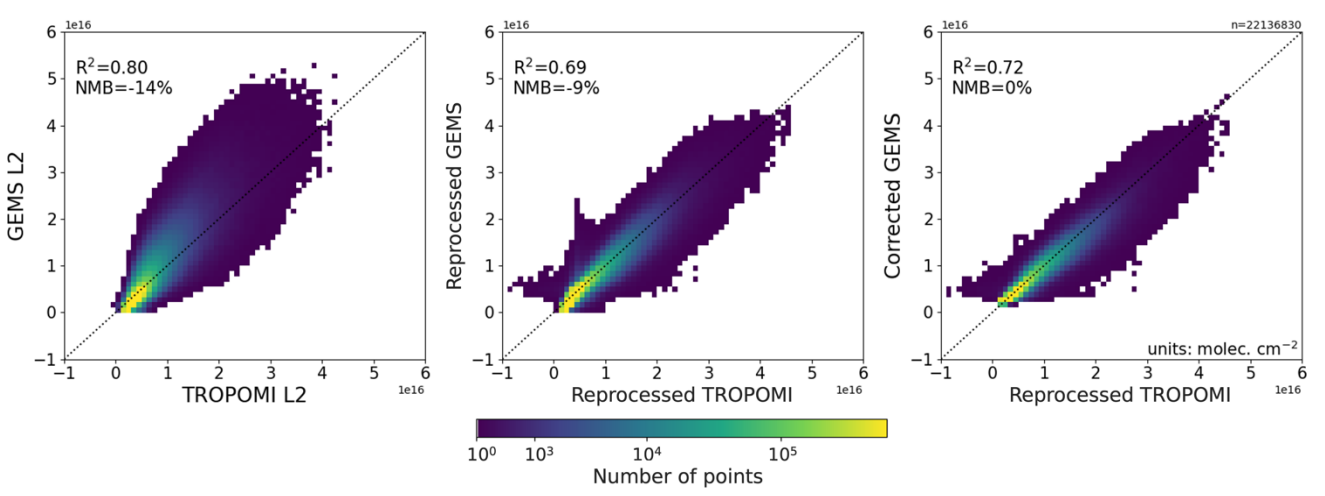

Figure 2: Scatterplot comparison of NO_2 VCDs from TROPOMI and GEMS. Individual points are daily data for July 2022−June 2023 on the 0.25° × 0.3125° grid sampled at the overpass time of TROPOMI. The left panel compares the operational TROPOMI and GEMS products and the middle panel compares our reprocessed products with GEOS-Chem NO_2 vertical profiles, respectively. The right panel compares the reprocessed TROPOMI product with the GEMS data corrected for residual differences with TROPOMI using machine learning (ML) (Section 4). Colorscale shows density of points. The dashed line indicates the 1:1 line. Coefficient of determination (R^2) and normalized mean bias (NMB) are given inset.

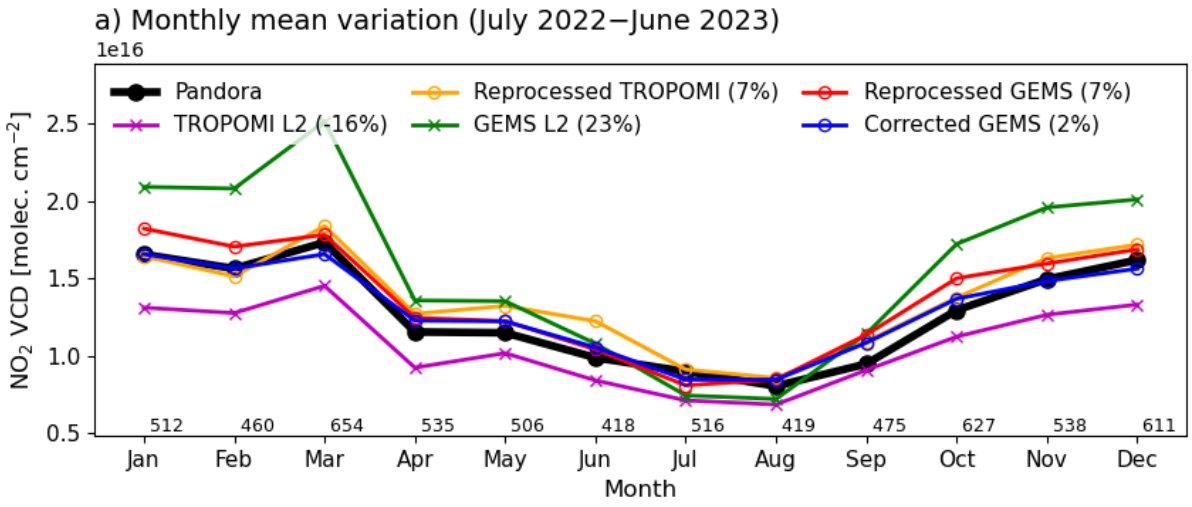
a) Monthly mean variation (July 2022−June 2023)
1e16
Pandora
TROPOMI L2 (-16%)
Reprocessed TROPOMI (7%)
GEMS L2 (23%)
Reprocessed GEMS (7%)
Corrected GEMS (2%)
NO2 VCD [molec. cm−2]
2.5
2.0
1.5
1.0
0.5
512
460
654
535
506
418
516
419
475
627
538
611
Jan
Feb
Mar
Apr
May
Jun
Jul
Aug
Sep
Oct
Nov
Dec
Month

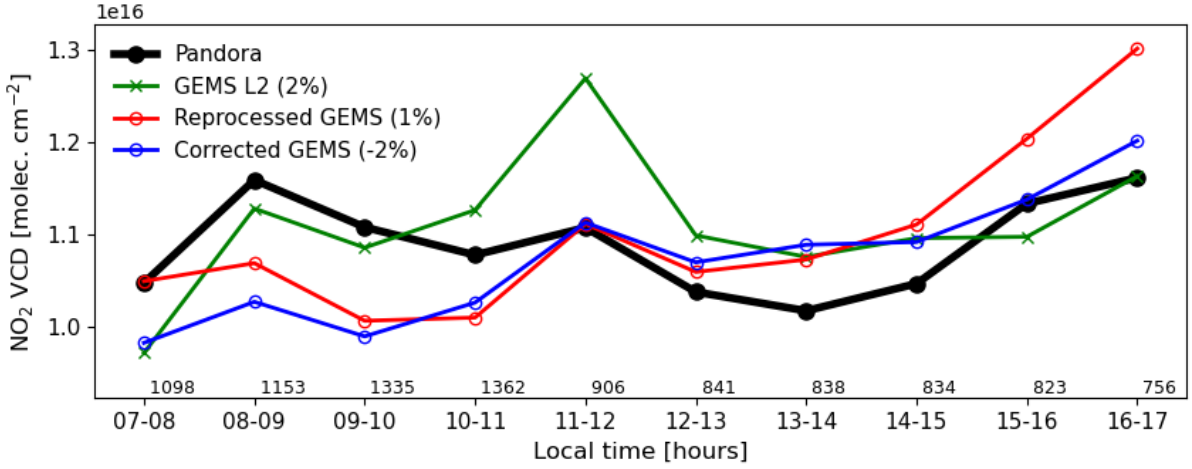
b) Hourly mean variation during warm months (April−September)
1e16
Pandora
GEMS L2 (2%)
Reprocessed GEMS (1%)
Corrected GEMS (-2%)
NO2 VCD [molec. cm−2]
1.3
1.2
1.1
1.0
1098
1153
1335
1362
906
841
838
834
823
756
07-08
08-09
09-10
10-11
11-12
12-13
13-14
14-15
15-16
16-17
Local time [hours]

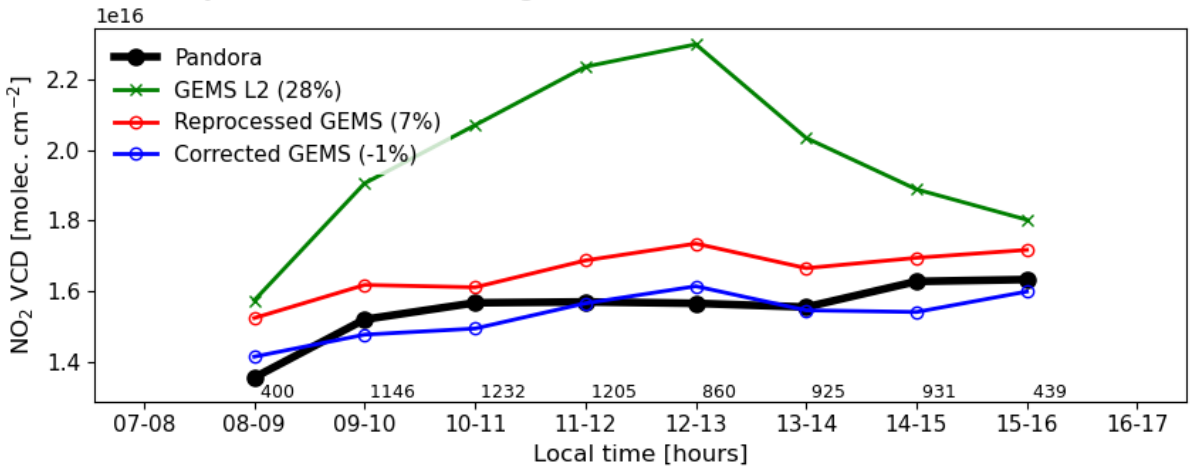
c) Hourly mean variation during cold months (October−March)
1e16
Pandora
GEMS L2 (28%)
Reprocessed GEMS (7%)
Corrected GEMS (-1%)
NO2 VCD [molec. cm−2]
2.2
2.0
1.8
1.6
1.4
400
1146
1232
1205
860
925
931
439
07-08
08-09
09-10
10-11
11-12
12-13
13-14
14-15
15-16
16-17
Local time [hours]

Figure 3: Seasonal and diurnal variations of NO_2 VCDs from Pandora, TROPOMI, and GEMS averaged at 15 Pandora stations in Northeast Asia over July 2022−June 2023. TROPOMI and GEMS data are shown for the operational L2 products, and the products reprocessed with GEOS-Chem NO_2 vertical profiles. Also shown is the GEMS product corrected for residual differences with TROPOMI using ML (Section 4). Seasonal variations in the top panel are for the TROPOMI overpass time (13:30 LT). Diurnal variations in the middle and bottom panels are only for Pandora and GEMS and are shown for April−September and October−March. NMB relative to Pandora are given inset. The numbers of observations for each month and hour are indicated.

a) SHAP analysis of predictor variables

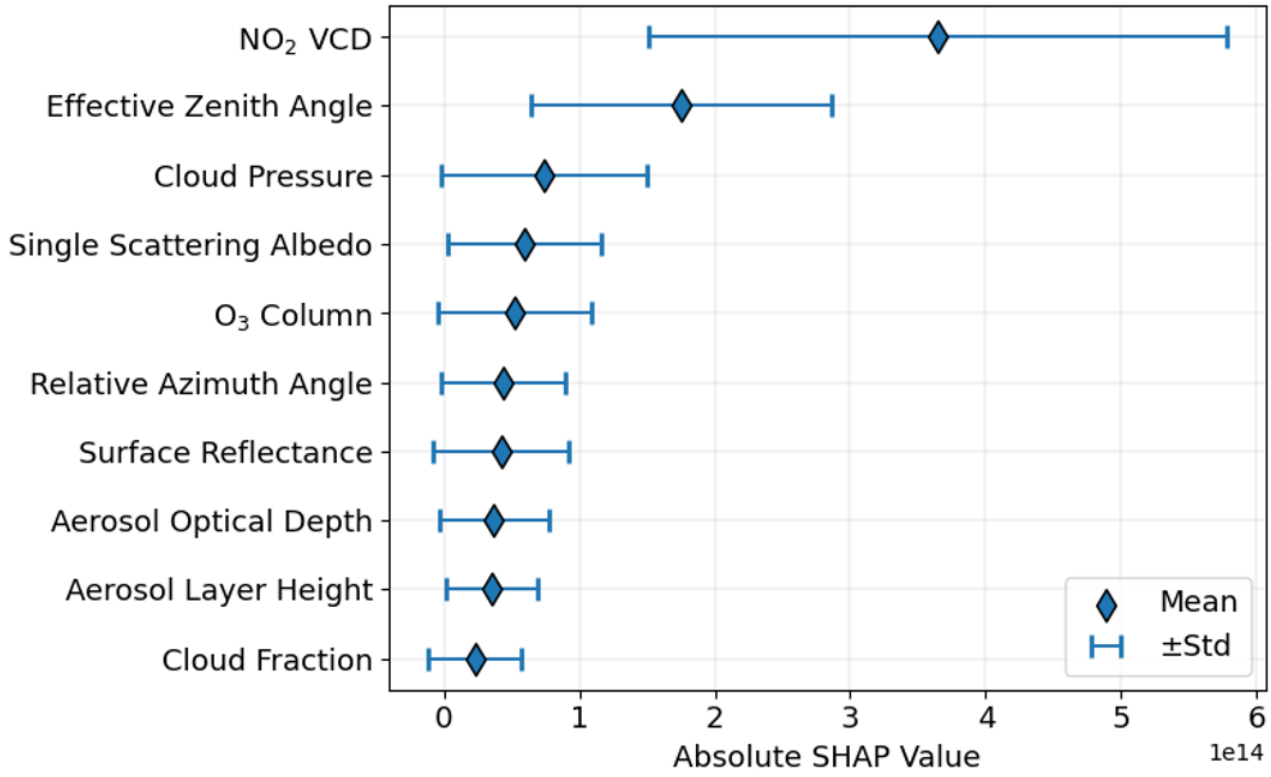

b) SHAP contribution to Δ(GEMS-TROPOMI)

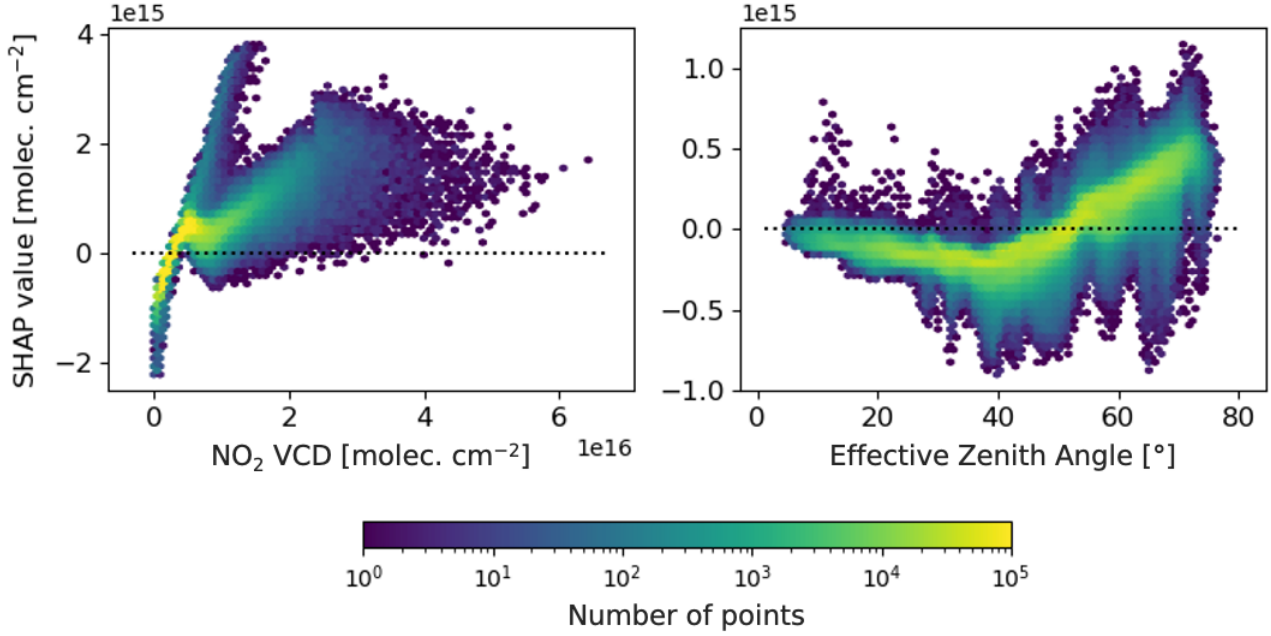

Figure 4: SHAP analysis for predictors of GEMS-TROPOMI differences, Δ(GEMS-TROPOMI), in the ML training dataset. (a) SHAP analysis results ranking the predictor variables in order of their contributions to the fit. (b) SHAP contribution to Δ(GEMS-TROPOMI) from GEMS NO_2 VCD and effective zenith angle (EZA). Colorscale shows density of points.

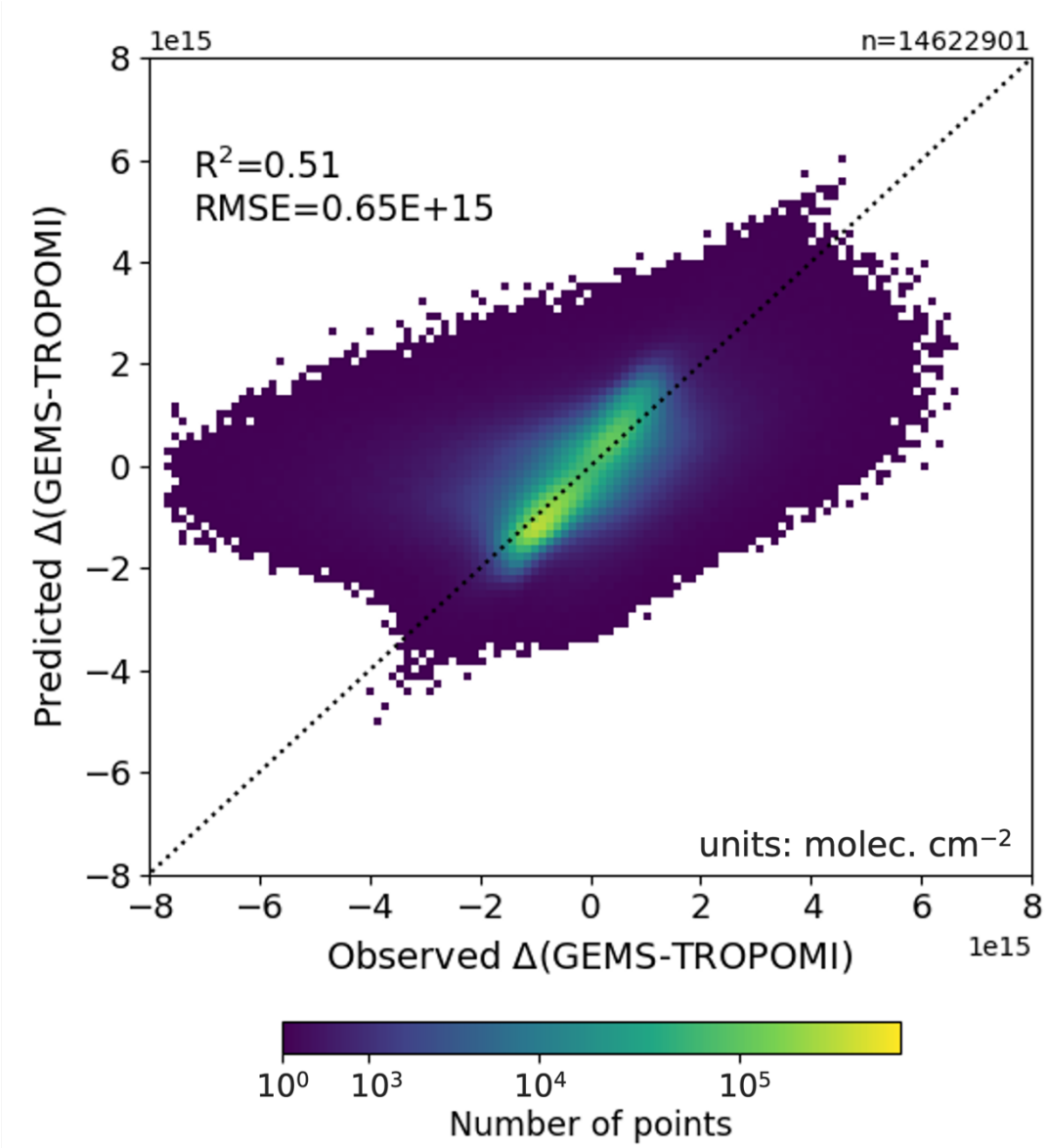

Figure 5: Predicted versus observed Δ(GEMS-TROPOMI) in the test dataset. Colorscale shows density of points. The dashed line indicates the 1:1 line. R^2 and root mean square error (RMSE) are given inset.

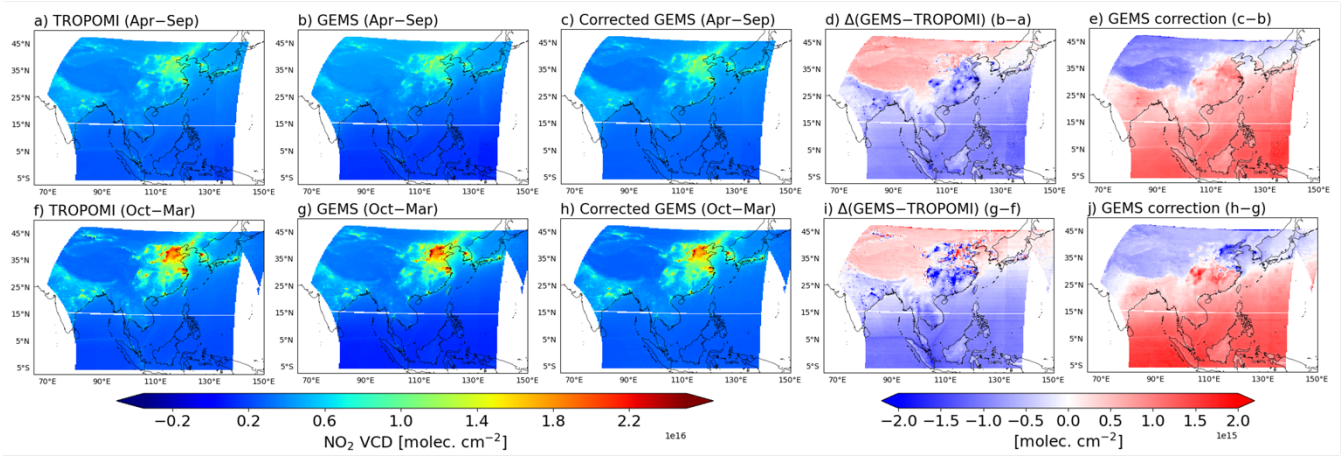

Figure 6: Comparison of TROPOMI, GEMS, and corrected GEMS NO_2 products in the GEMS scan domain. (a−c) NO_2 VCDs averaged for April–September at the TROPOMI overpass time. The TROPOMI and GEMS data have been reprocessed to common GEOS-Chem vertical profiles for the observation scenes. (d) Δ(GEMS-TROPOMI) for April–September. (e) Correction to the GEMS product for April–September. (f−j) Same as panels (a−e) but for October–March.

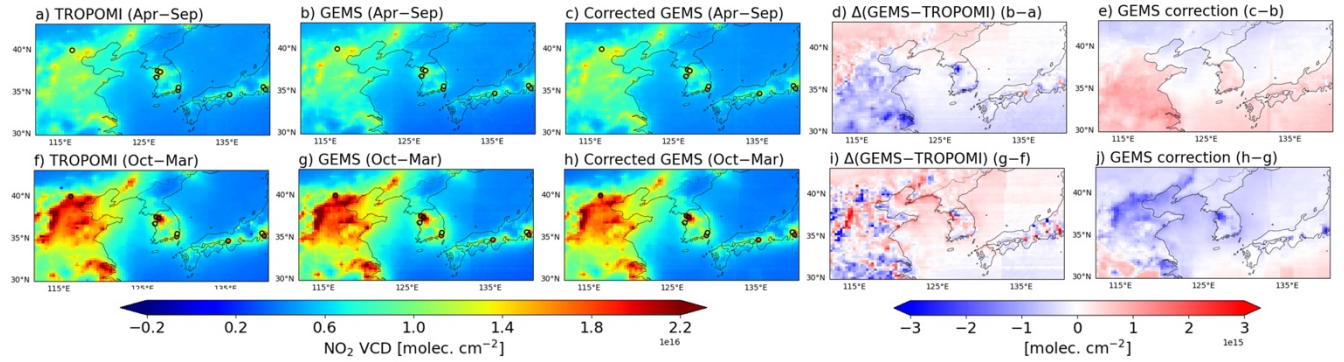

Figure 7: Same as Figure 6 but in the Northeast Asia domain with Pandora observations shown as circles. Colorscales are different from Figure 6.